# Effective Electrical Passivation of Ge(100) for HfO$_2$ Gate Dielectric Layers Using O$_2$ Plasma

**Qi Xie,[a] Davy Deduytsche,[a] Marc Schaekers,[b] Matty Caymax,[b,*]Annelies Delabie,[b,*] Xin-Ping Qu[c,*] and Christophe Detavernier[a,z]**

*[a]Department of Solid State Science, Ghent University, Krijgslaan 281/S1, B-9000 Ghent, Belgium*
*[b]IMEC, Kapeldreef 75, B-3001 Leuven, Belgium*
*[c]State Key lab of ASIC and System, Department of Microelectronics, Fudan University, Shanghai 200433, China*

The O$_2$ plasma pretreatment was investigated for passivation for HfO$_2$ high-$k$ Ge metal-oxide-semiconductor devices. With proper in situ O$_2$ plasma passivation, the capacitance–voltage hysteresis was substantially reduced from ∼900 to ∼50 mV for the HfO$_2$/Ge gate stacks. Capacitors show well-behaved capacitance–voltage characteristics on both p- and n-type Ge substrates, indicating an efficient electrical passivation of the Ge interface. The interface trap density for both types of Ge substrates after passivation is below $4 \times 10^{11}$ eV$^{-1}$cm$^{-2}$. A leakage current density of $1.5 \times 10^{-7}$ and $2.1 \times 10^{-8}$ A/cm$^2$ was obtained for the HfO$_2$/p-Ge and HfO$_2$/n-Ge capacitor with equivalent oxide thickness of 1.8 nm at V$_{FB} \pm 1$ V, respectively.

Continuous scaling of the complementary metal-oxide-semiconductor (CMOS) devices is pushing the traditional SiO$_2$ gate dielectric to a fundamental limit. Novel gate dielectric materials with a higher permittivity are in great demand in order to reduce the equivalent oxide thickness (EOT) and control the leakage current at acceptable level.[1] HfO$_2$ is a promising candidate for gate dielectric due to its relatively high dielectric constant, wide bandgap, and good thermal stability. Germanium (Ge) received an intensive interest because of improved electron (3900 vs 1400 cm$^2$/Vs) and hole (1900 vs 500 cm$^2$/Vs) bulk mobilities over Si.[2] However, one of the critical issues for Ge is the poor interface quality. Attempts at direct formation of a high-$k$ dielectric on Ge have not been successful.[3–5] Proper passivation of the Ge surface is required before it can be used as a channel material. Different approaches have been employed for Ge surface passivation including H$_2$O prepulsing,[6] thermal oxide treatment,[7–9] ozone oxidation,[10,11] atomic O beam,[12] epitaxial Si passivation,[13] and surface nitridation.[14] A relatively low interface trap density (to the low to mid of $10^{11}$ eV$^{-1}$cm$^{-2}$) was obtained for various dielectric including Al$_2$O$_3$, HfO$_2$, and ZrO$_2$. Promising electrical properties and small capacitance–voltage ($C$-$V$) hysteresis was achieved by adding an interlayer (IL) either GeON[15] or TaON[16] for HfO$_2$ dielectric while GeO$_2$ is commonly believed to be a poorly passivating oxide. In recent articles, it has been demonstrate that GeO$_2$ can also act as a promising electrical passivation layer for high-$k$ dielectric deposited by means of atomic layer deposition (ALD).[7,8] However, very large $C$-$V$ hysteresis (∼900 mV) was observed for the HfO$_2$ gate stack by using thermally grown GeO$_2$ passivation layer.[7,8] In previous literatures, excellent electrical characteristics in GeO$_2$/Ge MOS capacitors (MOSCAPs) grown by electron cyclotron resonance generated oxygen plasma were reported.[17] A high quality of germanium oxide was obtained by using atomic oxygen exposure.[18] However, GeO$_2$ exhibits a low dielectric constant (5–6)[19] and water solubility and, therefore, is not suitable to be used by itself as a gate dielectric. A combination of GeO$_2$ and a dielectric with higher $k$ value (e.g., HfO$_2$ or ZrO$_2$) is of great interest to obtain a low EOT and meet the requirements for future scaling. Recently, promising results were obtained for TiO$_2$ dielectric on Ge using ultrathin HfO$_2$/GeO$_2$ IL.[20] In this work, we investigate the HfO$_2$ gate dielectric on Ge and the GeO$_2$ passivation layer formed by remote radio frequency (rf) generated O$_2$ plasma. Air exposure was avoided between Ge passivation and subsequent ALD HfO$_2$ deposition. Interface trap density (D$_{it}$), fixed charge density, and gate leakage current density (J$_g$) were comprehensively evaluated for the MOSCAPs on both p- and n-type Ge substrates.

Ge(100) wafers (resistivity 0.05–0.1 Ω cm) were cleaned in a 0.5% HF solution followed by 5 min in deionized (DI) water. Then, the wafers were immediately loaded into the homebuilt ALD chamber through a loadlock. The details for the ALD setup were given in our previous work.[21,22] Prior to the HfO$_2$ deposition, Ge wafers were pretreated with surface oxidization at 250°C by using an O$_2$ plasma [remote inductively coupled plasma (ICP) source, downstream configuration]. The Ge wafers were exposed to the O$_2$ plasma at 200 W with a pressure around $1 \times 10^{-3}$ mbar, and the exposure time was varied from 30 to 60s. HfO$_2$ dielectric were subsequently grown by plasma-enhanced ALD (PE-ALD) with Tetrakis(ethylmethylamido)hafnium(IV) (TEMAH) and O$_2$ plasma at 250°C. Comparing to conventional thermal ALD, PE-ALD is considered a promising approach to deposit films at lower temperature with a high quality due to the higher reactivity of radicals. Additionally, degradation of hygroscopic GeO$_2$ IL was suppressed due to the absence of using H$_2$O when using PE-ALD. No air exposure for the samples during the O$_2$ plasma pretreatment and PE-ALD depositions. The samples remain stationary in the ALD chamber while the plasma source was separated from the ALD chamber through a computer controlled valve during the precursors pulse time to avoid contamination of the ICP source. A shadow mask was used to pattern the sputtered 50 nm thick Pt gate electrodes. A Ti(20 nm)/Pt(40 nm) bilayer structure was deposited as back electrode by sputtering. Postmetallization annealing (PMA) was conducted in a forming gas ambient at 350°C for 30 min before electrical measurements. The thickness of the films was measured both by ellipsometry and x-ray reflectivity (XRR). The chemical composition of the film was analyzed by depth profiling x-ray photoelectron spectroscopy (XPS) using Al Kα x-rays. The $C$-$V$ measurement was carried out using an HP 4192A impedance analyzer at various frequencies. The current was measured with a Keithley 617 electrometer, and the applied voltage to the capacitors was calibrated with a HP 3478A multimeter.

The $C$-$V$ hysteresis characteristics for the Pt/HfO$_2$/GeO$_2$/p-Ge MOSCAP without and with surface passivation are shown in Fig. 1. A very large $C$-$V$ hysteresis (∼900 mV) at flatband voltage was observed for the sample without surface passivation independent of the measured frequency (Fig. 1a), which is consistent with previous articles.[7] It is believed that the hysteresis is caused by the intermixing of GeO$_x$ and HfO$_2$. By using O$_2$ plasma pretreatment, much lower hysteresis (∼50 mV) was obtained although the HfO$_2$ deposition process is similar when compared to the MOSCAP without passivation. It might be due to the more uniform and stable GeO$_2$ IL
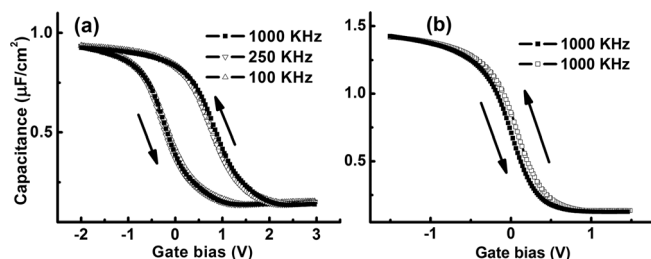
**Figure 1.** *C-V* hysteresis characteristics for $HfO_2$/p-Ge(100) gate stack with Pt as top electrode: (a) without $O_2$ plasma passivation and (b) with $O_2$ plasma passivation.
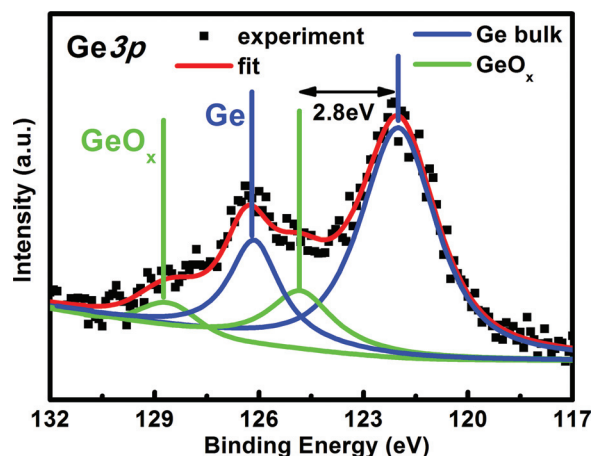


**Figure 2.** (Color online) XPS Ge 3p spectra at the $GeO_2$/Ge interface for the $HfO_2$/$GeO_2$/Ge stacks. Two components were extracted: Ge and $GeO_x$.

created by $O_2$ plasma treatment when it is conducted directly prior to the ALD process. For the MOSCAP without $O_2$ plasma pretreatment, the $O_2$ plasma during the initial ALD cycles may induce an intermixing reaction with the uncovered Ge surface and also the adsorbed TEMAH precursors (before the formation of a continuous $HfO_2$ film), which results in a nonuniform interface and more intermixing between $HfO_2$ and Ge substrate and, therefore, a larger *C-V* hysteresis.

The MOS devices properties on Ge are strongly correlated to the oxidation states of Ge at the interface. Complete Ge oxidation ($GeO_2$ or $Ge^{4+}$) at the interface is considered the best passivation IL. XPS results indicate a high quality of $GeO_2$ IL formed by $O_2$ plasma, evidenced by the chemical shift of $\sim$3.4 eV of Ge 3d referenced to Ge bulk and absence of apparent Ge suboxide contribution (not shown). Ge 3p has no overlap with Hf or O peaks and was, therefore, selected for XPS analysis for the samples after $HfO_2$ deposition.[7] The IL retains its $GeO_2$ nature mostly, and the atomic ratio of Ge/O at the interface is close to 1:2. A chemical shift of $\sim$2.8 eV was observed for the Ge 3p binding energy (BE) compared to the bulk Ge, as shown in Fig. 2. The shift is smaller than that for $Ge^{4+}$ (3 eV) while larger than $Ge^{3+}$ (2.5 eV), and the degradation is due to the subsequent $HfO_2$ deposition process, which caused partial intermixing of the $GeO_2$ and $HfO_2$.[7,11,12] However, the degradation is not significant because the decrease of BE shift is only $\sim$0.2 eV. XPS measurement also shows the atomic concentration of Ge in $HfO_2$ films is less than 3%, which indicates a sufficient suppression of Ge outdiffusion by using rf-$GeO_2$ and in situ PE-ALD $HfO_2$. This observation is consistent with small *C-V* hysteresis properties—large hysteresis is usually caused by the bulk oxide traps related to Ge outdiffusion.[7,8,12]

MOSCAPs with various thicknesses (3–18 nm) of $HfO_2$ were fabricated, and capacitance at strong accumulation was measured for the MOSCAPs with passivation (data not shown). EOT was extracted by fitting the *C-V* characteristics based on the Ge-simulator, taking the quantum-mechanical effect into consideration. Based on the equation $EOT = t_{IL} + (k_{SiO_2}/k_{ox})t_{ox}$, extrapolation suggests a relative dielectric constant of $HfO_2$ $k_{ox}$ is $\sim$24 and the EOT contributed from the $GeO_2$ interlayer $t_{IL}$ is $\sim$1 nm, which gives the physical

thickness of $GeO_2$ around 1.4–1.5 nm, considering the $GeO_2$ dielectric constant of $\sim$5.6.[19] It is worth mentioning that the $HfO_2$ film grown by thermal ALD (using $H_2O$) exhibits a lower *k* value of $\sim$18.

Figure 3 shows the *C-V* characteristics of the Pt/$HfO_2$/$GeO_2$/Ge MOSCAPs measured at different frequencies (200 Hz to 1000 KHz) on both p- and n-type Ge(100). The thickness of $HfO_2$ is around 5 nm for both stacks. EOT increased around 15% after annealing in forming gas anneal (FGA) ambient at 350°C for 30 min. Well-behaved *C-V* curves are observed for both gate stacks without significant frequency dispersion, stretch out, or bumps in the depletion region. The *C-V* characteristics also show evidence of inversion with a minority carrier response at a low frequency and a flat $C_{min}$ at a high frequency. This indicates the efficient electrical passivation of the Ge interface. It should be noted that an inversion layer was formed at relatively high frequency (1 kHz) compared to Si. This is related to the short minority carrier response time in Ge, which is related to the small bandgap of Ge ($\sim$0.66 eV). It has been reported previously that the transition frequency from low frequency to high frequency behavior is around 6 kHz for Ge, which is about 2 orders of magnitude higher than Si MOSCAP ($\sim$70 Hz).[23] $D_{it}$ was calculated based on the high-low frequency,[24] and the Berglund integral method was used to relate the gate voltage to the corresponding surface potential.[25] The plots for the $D_{it}$ obtained by this method are shown in the inset of Fig. 3. It was limited in the depletion region to avoid the weak inversion response. The $D_{it}$ at flatband condition is $3.3 \times 10^{11}$ $eV^{-1}cm^{-2}$ and $3.7 \times 10^{11}$ $eV^{-1}cm^{-2}$ for the $HfO_2$/$GeO_2$/p-Ge and the $HfO_2$/$GeO_2$/n-Ge MOSCAPs, respectively. It shows substantially a lower $D_{it}$ comparing to the $GeO_xN_y$ IL formed by in situ $NH_3$ plasma ($\sim$6 $\times 10^{11}$ $eV^{-1}cm^{-2}$) although the subsequent $HfO_2$ deposition is identical.[26]

Figure 4 represents the surface potential of $HfO_2$/$GeO_2$/Ge stacks, extracted by the Berglund method for both p- and n-Ge(100).



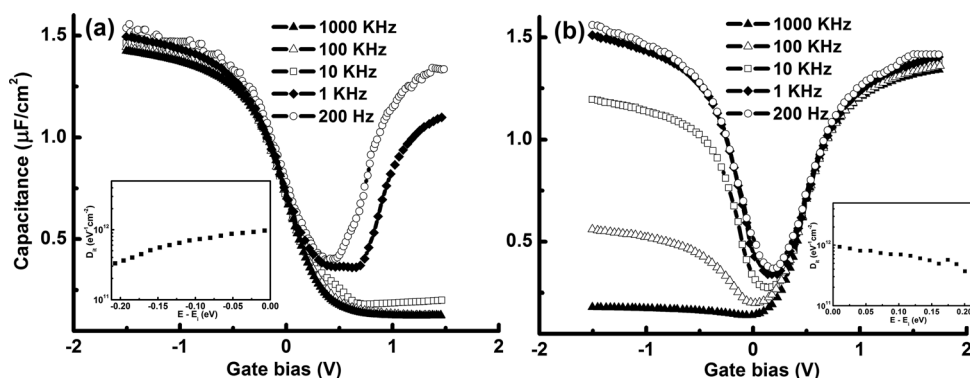**Figure 3.** *C-V* characteristics of $HfO_2$ on Ge(100) substrate with $O_2$ plasma passivation measured at various frequencies: (a) $HfO_2$/$GeO_2$/p-Ge and (b) $HfO_2$/$GeO_2$/n-Ge MOSCAPs. The thickness of $HfO_2$ and $GeO_2$ is $\sim$5 and 1.4 nm, respectively. The insets show the energy distribution of the $D_{it}$ for both the MOSCAPs.
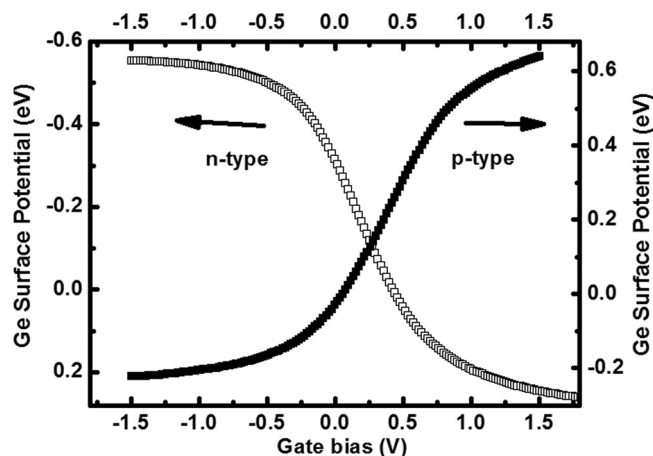
**Figure 4.** Surface potential as a function of gate bias for both types of capacitors.

The modulation of surface potential with the gate bias indicates that the Fermi level at the surface is swept through the entire Ge bandgap ($\sim$0.66 eV), which indicates that the Ge surface is unpinned. The effective workfunction of the gate electrode in the MOS stack can be extracted by estimating the flatband voltage for a series of capacitors with various EOT. Under conditions of minimal bulk dielectric charge, a plot of $V_{FB}$ vs EOT is supposed to follow the relation $q\,V_{FB} = \phi_{ms} - (Q_{fix} \times EOT)/\varepsilon_{ox}$, where the slope ($Q_{fix}$) is the fixed charge density at the dielectric/semiconductor interface, and the linear intercept ($\phi_{ms}$) is the metal/semiconductor workfunction difference. Extrapolation (data not shown) suggests fixed charge densities around $3 \times 10^{12}$ cm$^{-2}$ and an effective workfunction of Pt of $\sim$4.8 eV.

Figure 5 shows the comparison of the $J_g$ as a function of EOT according to the published data and this work. A $J_g$ of $1.5 \times 10^{-7}$ A/cm$^2$ and $2.1 \times 10^{-8}$ A/cm$^2$ was obtained for the HfO$_2$/p-Ge and HfO$_2$/n-Ge capacitors with EOT of 1.8 nm at $V_{FB}\pm 1$ V, respectively. With the decreasing thickness of HfO$_2$ and GeO$_2$, an EOT of 1.3 nm and $J_g$ of $1 \times 10^{-6}$ A/cm$^2$ at $V_{FB}\pm 1$ V were achieved. A low $J_g$ indicates a high quality of the HfO$_2$ films deposited by PE-ALD compared to other process. Hf 4f XPS spectra are investigated, and stoichiometric HfO$_2$ was obtained by PE-ALD without a significant binding energy shift or defects. XRR results suggest that the density of the HfO$_2$ approaches its bulk value. High density and high quality of HfO$_2$ films grown by PE-ALD are related to the highly reactive O radicals and the absence of H$_2$O during the ALD process, which avoids degradation of the GeO$_2$ IL during
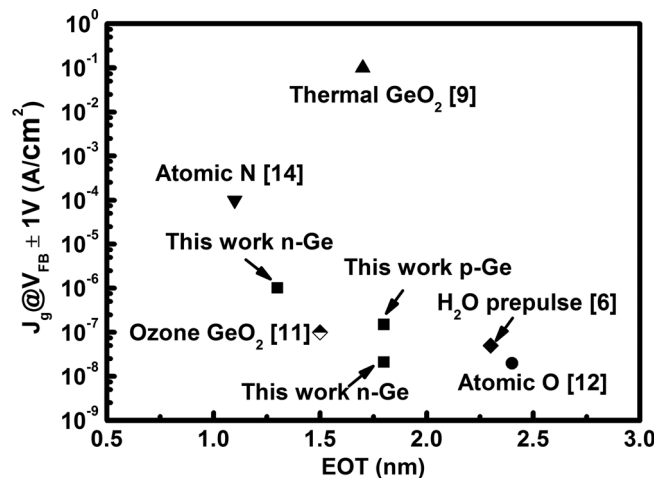
the ALD growth. A comparison of the HfO$_2$ dielectrics grown with both thermal ALD (using H$_2$O) and PE-ALD on the identical GeO$_2$ IL formed by in situ O$_2$ plasma treatment was conducted. Substantially a higher *C-V* hysteresis (250 vs 50 mV) and also a lower dielectric breakdown was observed for the capacitor with the thermally grown HfO$_2$ compared to the PE-ALD grown HfO$_2$, although the GeO$_2$ IL was identical.

To conclude, the MOSCAPs demonstrate a very promising comprehensive device performances including excellent *C-V* characteristics on both p- and n-type Ge(100), small *C-V* hysteresis, low $D_{it}$, and low $J_g$. The good overall behavior is due to the combinations of three factors, i.e., high quality of GeO$_2$ formed by O$_2$ plasma, high quality of HfO$_2$ grown by PE-ALD, and absence of air exposure (i.e., in situ).

## References

1. G. D. Wilk, R. M. Wallace, and J. M. Anthony, *J. Appl. Phys.*, **89**, 5243 (2001).
2. C. O. Chui, H. Kim, D. Chi, B. B. Triplett, P. C. McIntyre, and K. C. Saraswat, *Tech. Dig. - Int. Electron Devices Meet.*, **2002**, 437.
3. C. O. Chui, S. Ramanathan, B. B. Triplett, P. C. McIntyre, and K. C. Saraswat, *IEEE Electron Device Lett.*, **23**, 473 (2002).
4. E. P. Gusev, H. Shang, M. Copel, M. Gribeyuk, C. D. Emic, P. Kozlowski, and T. Zabel, *Appl. Phys. Lett.*, **85**, 2334 (2004).
5. D. S. Yu, K. C. Chiang, C. F. Cheng, A. Chin, C. Zhu, M. F. Li, and D. L. Kwong, *IEEE Electron Device Lett.*, **25**, 559 (2004).
6. S. Swaminathan, Y. Oshima, M. A. Kelly, and P. C. McIntyre, *Appl. Phys. Lett.*, **95**, 032907 (2009).
7. A. Delabie, F. Bellenger, M. Houssa, T. Conard, S. V. Elshocht, M. Caymax, M. Heyns, and M. Meuris, *Appl. Phys. Lett.*, **91**, 082904 (2007).
8. F. Bellenger, M. Houssa, A. Delabie, V. Afanasiev, T. Conard, M. Caymax, M. Meuris, K. D. Meyer, and M. M. Heyns, *J. Electrochem. Soc.*, **155**, G33 (2008).
9. K. Kutsuki, G. Okamoto, T. Hosoi, T. Shimura, and H. Watanabe, *Appl. Phys. Lett.*, **95**, 022102 (2009).
10. D. Kuzum, T. Krishnamohan, A. J. Pethe, A. K. Okyay, Y. Oshima, Y. Sun, J. P. McVittie, P. A. Pianetta, P. C. McIntyre, and K. C. Saraswat, *IEEE Electron Device Lett.*, **29**, 328 (2008).
11. A. Delabie, A. Alian, F. Bellenger, M. Caymax, T. Conard, A. Franquet, S. Sioncke, S. Elshocht, M. M. Heyns, and M. Meuris, *J. Electrochem. Soc.*, **156**, G163 (2009).
12. P. Tsipas, S. N. Volkos, A. Sotiropoulos, S. F. Galata, G. Mavrou, D. Tsoutsou, Y. Panayiotatos, A. Dimoulas, C. Marchiori, and J. Fompeyrine, *Appl. Phys. Lett.*, **93**, 082904 (2008).
13. M. Caymax, F. Leys, J. Mitard, K. Martens, L. Yang, G. Pourtois, W. Vandervorst, M. Meuris, and R. Loo, *J. Electrochem. Soc.*, **156**, H979 (2009).
14. J. J. H. Chen, N. A. Bojarczuk, H. Shang, M. Copel, J. B. Hannon, J. Karasinski, E. Preisler, and S. K. Banerjee, *IEEE Trans. Electron Devices*, **51**, 1441 (2004).
15. C. O. Chui, H. Kim, P. C. McIntyre, and K. C. Saraswat, *IEEE Electron Devices Lett.*, **25**, 274 (2004).
16. T. Sugawara, Y. Oshima, R. Sreenivasan, and P. C. McIntyre, *Appl. Phys. Lett.*, **90**, 112912 (2007).
17. Y. Fukuda, T. Ueno, S. Hirono, and S. Hashimoto, *Jpn. J. Appl. Phys.*, 44, 6981 (2005).
18. A. Molle, M. N. K. Bhuiyan, G. Tallarida, and M. Fanciulli, *Appl. Phys. Lett.*, **89**, 083504 (2006).
19. S. Takagi, T. Maeda, N. Taoka, M. Nishizawa, Y. Morita, K. Ikeda, Y. Yamashita, M. Nishikawa, H. Kumagai, and R. Nakane, *Microelectron. Eng.*, **84**, 2314 (2007).
20. Q. Xie, D. Deduytsche, M. Schaekers, M. Caymax, A. Delabie, X. P. Qu, and C. Detavernier, *Appl. Phys. Lett.*, **97**, 112905 (2010).
21. Q. Xie, Y. L. Jiang, C. Detavernier, D. Deduytsche, R. L. Van Meirhaeghe, G. P. Ru, B. Z. Li, and X. P. Qu, *J. Appl. Phys.*, **102**, 083521 (2007).
22. Q. Xie, J. Musschoot, D. Deduytsche, R. L. Meirhaeghe, C. Detavernier, S. Berghe, Y. L. Jiang, G. P. Ru, B. Z. Li, and X. P. Qu, *J. Electrochem. Soc.*, **155**, H688 (2008).
23. A. Dimoulas, G. Vellantis, G. Mavrou, E. K. Evangelou, and A. Sotiropoulos, *Appl. Phys. Lett.*, **86**, 223507 (2005).
24. D. K. Schroder, *Semiconductor Material and Device Characterization*, pp. 337–419, John Wiley & Sons, New York (1998).
25. C. N. Berglund, *IEEE Trans. Electron Devices*, **13**, 10 (1966).
26. Q. Xie, J. Musschoot, M. Schaekers, M. Caymax, A. Delabie, X. P. Qu, Y. L. Jiang, S. V. D. Berghe, J. Liu, and C. Detavernier, *Appl. Phys. Lett.*, **97**, 222902 (2010).

**Figure 5.** Comparison of $J_g$ at $V_{FB} \pm 1$ V with respect to different EOTs according to the published data and this work.